Mechanistic aspects of n-hexadecane hydroconversion

Fuel 358 (2024) 130264

Contents lists available at ScienceDirect

Fuel

journal homepage: www.elsevier.com/locate/fuel

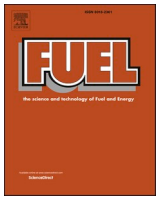

Full Length Article

Mechanistic aspects of n-hexadecane hydroconversion: Impact of di-branched isomers on the cracked products distribution

Douglas Romero [a], Marcello Rigutto [b], Emiel J.M. Hensen [a,*]

[a] Laboratory of Inorganic Materials and Catalysis, Department of Chemical Engineering and Chemistry, Eindhoven University of Technology, P.O. Box 513, 5600 MB Eindhoven, the Netherlands
[b] Shell Global Solutions International B.V., P.O. Box 38000, 1030 BN Amsterdam, the Netherlands

ARTICLE INFO

Keywords:
Hydrocracking
Zeolite
Mesoporous silica
Mechanism
Product distribution

ABSTRACT

The mechanism of n-hexadecane (n-C_{16}) hydroisomerization/hydrocracking was studied over bifunctional catalysts employing Pd and Pt as (de)hydrogenation components and large-pore zeolites and (ordered) mesoporous materials as acidic supports. Zeolite Y and Beta supports were compared to amorphous silica-alumina as well as aluminium-containing ordered mesoporous MCM-41, MCM-48 and SBA-15 materials to cover a wide range of pore sizes and topologies. Products were analyzed in terms of mono- and di-branched C_{16} isomers and cracked products as a function of the n-C_{16} conversion. All samples followed a similar mechanism in which, at low conversion, di-branched isomers with methyl groups toward the ends of the tetradecane chain were observed. At higher conversion, the products shifted to isomers with methyl groups closer to the center at higher n-C_{16} conversion. Consistent with these differences, the typical 'M' shape distribution of cracked products was obtained at low conversion, which evolved into ideal symmetric cracking patterns at higher conversion. The unusual di-branched isomer distribution at low conversion and the corresponding 'M' shaped cracked products distribution have earlier been associated with pore mouth catalysis induced by restricted diffusion in medium-pore zeolites. Here we show that such reaction pathways also occur in catalysts with large enough pores to exclude diffusion restrictions.

1. Introduction

Hydroconversion of long-chain paraffins has gained significant relevance in the chemical industry, because high-quality transportation fuels can be obtained from a variety of feedstocks, including heavy fractions of crude oil, Fischer-Tropsch waxes and vegetable oils [1]. The process encompasses hydroisomerization and hydrocracking of linear paraffins. The first reaction comprises skeletal isomerization with limited cracking and is employed to increase the octane number of gasoline and achieve better cold-flow properties of kerosene and diesel. In the second reaction, heavy (gas oil) hydrocarbons are cracked into more valuable diesel fuel by reducing their carbon number. For hydroconversion, bifunctional catalysts containing noble metals like Pd or Pt are combined with acidic zeolite or amorphous silica-alumina, reflecting hydrogenation/dehydrogenation (metal component) and isomerization/cracking (Brønsted acid component) functions, respectively [2].

Although the hydroconversion of n-paraffins has been extensively studied for several decades, it is still not completely understood how the catalytic mechanism proceeds and how the product distribution relates to the textural properties of the porous acid catalysts. In general, two mechanisms have been considered. The most widely accepted one, known as the classical mechanism [3,4], involves the dehydrogenation of n-alkanes on metal sites to corresponding n-alkenes, which are then transported to Brønsted acid sites (Fig. 1). Alkoxy species obtained upon protonation can undergo reactions such as skeletal rearrangement (methyl and ethyl branching, hydride and alkyl shifts) and ß-scission (carbon–carbon bond cleavage) reactions, which are thought to proceed via transition states that have a carbenium ion character. The rate of the important ß-scission step depends on the degree of isomerization of the carbenium ion. Intermediates with a higher branching degree will crack faster. As such, the cracking steps can be arranged in terms of rates from fastest to slowest as type A (formation of tertiary carbenium ion from a tertiary carbenium ion) > type B (tertiary (or secondary) ion from secondary (or tertiary) ion) > type C (secondary-to-secondary carbenium ion cracking) [5]. Cracking via primary carbenium ions proceeds very slowly. The reaction cycle is closed by alkene desorption from acid sites

* Corresponding author.
E-mail address: e.j.m.hensen@tue.nl (E.J.M. Hensen).

https://doi.org/10.1016/j.fuel.2023.130264
Received 4 September 2023; Received in revised form 13 October 2023; Accepted 30 October 2023
Available online 11 November 2023

and formation of the corresponding alkane upon hydrogenation on metal sites. The relative location of metal and acid functions and intermediates desorption and diffusion can also play an important role in determining the product distribution. This has been early described by the concept of "intimacy", which refers to the condition of close proximity between metal and acid sites. The intimacy criterion defined by Weisz [6] refers to the maximum distance between these types of sites beyond which a decrease of catalytic activity is observed.

Some recent studies have revisited the intimacy concept, employing physically mixtures of acid components (USY [7], HZSM-22 [8], ZSM-5/Beta [9], or SBA-15 [10]) with Al_2O_3 as support, in which the metal function is either placed on the acidic solids (Pt/Ac) or on the alumina (Pt/Al). As can be expected, the similar acidity of the Pt/Ac and Pt/Al composite catalysts led to similar hydroconversion activity for the same type of acidic support. The Pt/Al composites led to higher isomerization yields (and thus lower cracking yields) for Pt/Al catalysts in comparison to catalyst where the Pt particles were inside the zeolite pores where also the acid sites reside [11]. These findings indicate that close proximity of the metal and acid sites can be unfavourable and that higher isomerization yields can be obtained by separating these two functions [7]. The explanation postulated by the authors centers around predominant reaction of the olefinic intermediates in the outer regions of the zeolite crystals, allowing rapid diffusion back to the metal sites on Al_2O_3, which is seemingly in line with the concept of pore-mouth catalysis [12].

In this work, we investigated n-hexadecane (n-C_{16}) hydroconversion employing palladium and platinum-palladium catalysts supported on zeolite (Beta, Y), amorphous silica-alumina (ASA) and ordered mesoporous silica modified by Al (SBA-15, MCM-41, MCM-48) with significant textural and compositional (Si/Al ratios) differences of the acid support materials. These materials were characterized for their basic physicochemical properties including metal dispersion and acidity. The products of n-C_{16} were analyzed in detail in terms of mono-branched and di-branched C_{16} isomers in order to understand the relation with the distribution of cracked products. Complementary n-heptane (n-C_7) hydroconversion experiments for some catalysts are reported as well.

2. Experimental methods

2.1. Catalyst preparation

Siliceous MCM-41 sample was prepared by dissolving 3.8 g tetramethyl ammonium hydroxide solution (TMAOH, 25 % wt in water) and 4.6 g cetyltrimethyl ammonium bromide (CTAB) in 34.1 g water. After stirring at 308 K for 1 h, 3.0 g fumed silica was added and the gel was further stirred at room temperature for 20 h. The gel was transferred to a Teflon-lined stainless-steel autoclave and heated at 423 K for 48 h.

Siliceous MCM-48 sample was synthesized by dissolving 2.14 g fumed silica in 30 g a 10 wt% cetyltrimethylammonium hydroxide solution in water (CTAOH). After stirring at room temperature for 2 h, the gel was transferred to a Teflon-lined stainless-steel autoclave and heated at 408 K for 24 h.

SBA-15 with a target Si/Al ratio of 20 was synthesized employing a hydrochloric acid solution of pH 1.7. Solution A was prepared by dissolving 2 g Pluronic P123 in 70 ml in the acid solution followed by stirring at 313 K for 6 h. A second solution B was obtained by dissolving 0.22 g aluminum triisopropoxide and 3.2 ml tetramethylorthosilicate (TMOS) in 5 ml of the acid solution, followed by stirring at room temperature for 2 h. Solution B was then added to solution A, followed by further stirring at 313 K for 20 h. The resulting suspension was transferred to a Teflon-lined stainless-steel autoclave, which was then sealed and heated at 373 K for 48 h.

After the hydrothermal synthesis step, the solids were filtrated and washed with deionized water. All of these samples were dried overnight at 373 K and the template was removed in a next step by calcination at 773 K for 10 h (SBA-15) and 823 K for 6 h (MCM-41 and MCM-48).

The siliceous MCM-41 and MCM-48 samples were aluminated by a dry alumination method. For this purpose, 2.0 g calcined MCM-41 was dispersed in 50 ml of dry n-hexane. Solutions containing 0.11 g aluminum triisopropoxide in 150 ml of n-hexane were prepared to obtain materials with Si/Al ratios of 60. The MCM-41 suspension was added to the aluminum-containing solution and the mixture was stirred at room temperature for 24 h. For MCM-48, 1 g of the mesoporous silica

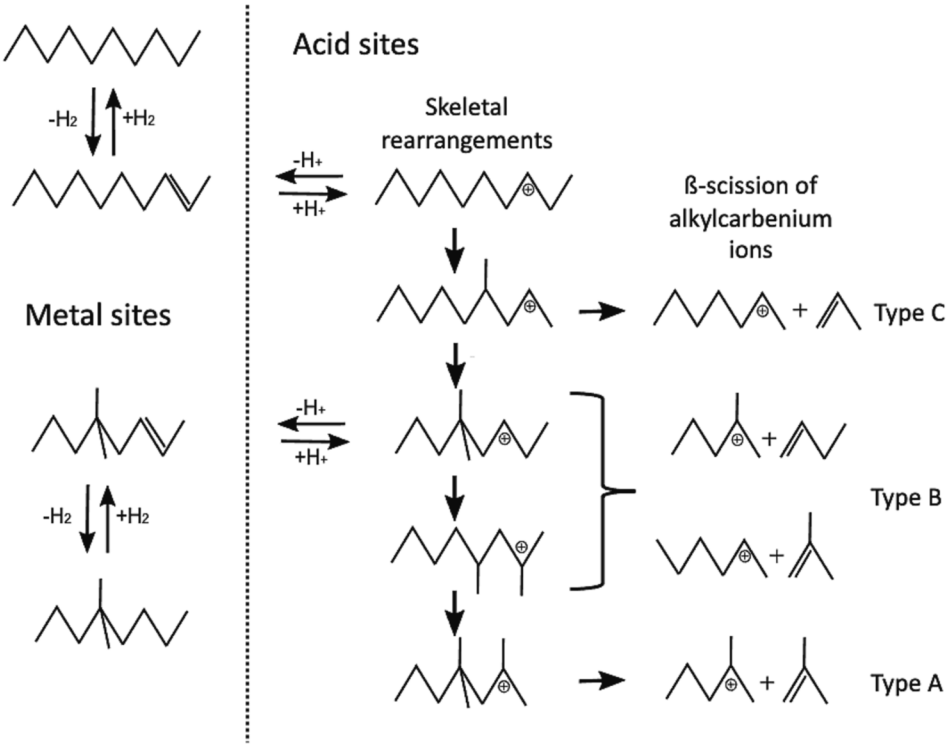

Fig. 1. Classical mechanism of hydroisomerization and hydrocracking.

was added to a solution containing 0.06 g of aluminum isopropoxide in 50 ml of n-hexane and the resulting dispersion was further stirred at room temperature for 24 h to obtain a Si/Al ratio of 60. The solids were recovered by filtration and washed with n-hexane. The samples were dried overnight at 373 K and subsequently calcined at 823 K for 4 h.

Commercial ultrastabilized Y (USY), Beta and ASA (amorphous silica-alumina, 75/25 w/w from JGC) were used as received.

The solid acid support materials were loaded with 1 wt% Pd by wet impregnation with an aqueous $Pd(NH_3)_4(NO_3)_2$ solution. The resulting samples were calcined at 723 K (rate 0.5 K/min) in flowing air for 4 h. 0.5 wt% Pt – 1 wt% Pd catalysts were obtained by a follow-up impregnation of the original Pd-Beta and Pd-SBA-15 catalysts with an aqueous $H_2PtCl_6{*}6H_2O$ solution. The samples were subsequently calcined at 723 K (rate 0.5 K/min) in flowing air for 4 h.

2.2. Catalytic activity measurements

For n-C_{16} hydroconversion activity measurements, the catalyst was first loaded into the reactor and dried at 1 bar and 473 K for 1 h in a He flow followed by reduction at 60 bar in a H_2 flow. For reduction, the temperature was increased at a rate of 3 K/min to 673 K followed by an isothermal period of 1 h. Then, the temperature of the catalyst bed was lowered to 473 K and the packed bed was wetted by maintaining a liquid flow rate of 1 ml/min for 10 min. The reactor was operated at a H_2/n-hexadecane molar ratio of 20 and a weight hourly space velocity (WHSV) of 10 $g_{n\text{-}C16}\ g_{cat}^{-1}h^{-1}$. The reaction temperature was increased stepwise and the reaction was equilibrated for 3 h before product sampling. The reactor effluent was analyzed by a gas chromatograph equipped with an RTX-1 column and a flame ionization detector.

For n-C_7 hydroconversion, the Pd-containing zeolite catalysts were pressed, crushed and sieved into a 177–420 μm particle fraction. Prior to activity testing, the catalysts were reduced at 440 °C and under 30 bar flowing H_2. The catalytic activity measurements were carried out at 30 bar, a molar H_2/n-heptane ratio of 24 and a gas hourly space velocity (GHSV) of 15,000 $Nml_{n\text{-}C7}\ g_{cat}^{-1}h^{-1}$. The initial reaction temperature was 440 °C. Then, the temperature was lowered at a rate of 0.2 °C /min to 170 °C.

3. Results and discussion

Basic characterization of the catalysts (Table S2) shows that the Pd loading is close to the targeted 1 wt%. For the sample to which Pt was added in a second impregnation step, the Pt loading was close to the intended 0.5 wt%. As expected, the zeolite supports present much higher acidity than the other samples, in line with the concentration of BAS determined by H/D exchange and FTIR of adsorbed pyridine (Table S1). Based on H_2 chemisorption, the metal nanoparticles are in the range of 2–10 nm. Pore size distributions (Figure S1) show the wide range of pores sizes covered by the porous solid acids, from the typical pore size of 0.55 nm of Beta zeolite [13] to cylindrical pores of around 9 nm in SBA-15 [14]. X-ray diffractograms exhibit the expected patterns for the various materials (Figure S3). Specifically, we observe the (111), (331) and (533) lines of zeolite Y [15], the (101) and (300) lines of zeolite Beta [16], the (100), (110), (200) and (210) lines of the hexagonal *p6mm* structure of MCM-41 [17], the (211), (220) and (420) lines of the cubic *Ia3d* structure of MCM-48 [18], and the (100), (110) and (200) lines of the hexagonal *p6mm* structure of SBA-15 [19].

The ratio between available metal sites and Brønsted acid sites is sufficiently high for all samples to ensure that acid-catalyzed reactions control the overall reaction rate [20]. The catalytic performance of the Pd and Pt-Pd loaded catalysts for n-C_{16} hydroconversion was evaluated at a weight hourly velocity of 10 $g_{n\text{-}C16}\ g_{cat}^{-1}h^{-1}$, a total pressure of 60 bar and a H_2/n-hexadecane ratio of 20. The n-C_{16} conversion is shown as function of the temperature in Fig. 2. Among the Pd samples, the zeolite-supported catalysts are substantially more active than the catalysts based on amorphous supports. This difference becomes smaller, considering that the n-C_{16} conversion of the Pd-SBA-15 sample increases considerably after addition of Pt. Fig. 2 also shows that Pd-ASA, Pd-Beta, Pt-Pd-Beta and Pt-Pd-SBA-15 are highly selective to C_{16} isomerization products. Maximum isomerization yields decrease in the order Pd-ASA > Pd-Beta ≈ Pt-Pd-Beta ≈ Pt-Pd-SBA-15 > Pd-SBA-15 ≈ Pd-MCM-41 > Pd-MCM-48 > Pd-Y. Adding Pt to the Pd-SBA-15 catalyst results in a higher yield of C_{16} isomers for Pt-Pd-SBA-15. The higher activity and selectivity to isomers upon Pt addition indicates that the supply of olefins to the acid sites is limiting the catalytic performance of Pd-SBA-15 (Figure S6).

The average number of acid-catalyzed steps (n_{as}) was calculated following the procedure reported by Batalha et al. [21,22]. This involves the extrapolation of the product distribution to zero reactant (i.e., n-C_{16}) conversion and the consideration that under ideal hydrocracking conditions mono-branched isomers are obtained by one acid-catalyzed step per dehydrogenation/hydrogenation event, di-branched isomers by two acid-catalyzed steps and so forth. The values of the average number of acid-catalyzed steps during n-C_{16} conversion obtained in this way lie between 1.32 and 1.70 for the investigated catalysts. From this, we can conclude that there is no substantial effect of shape selectivity for these composite catalysts, as catalysts with strong shape selectivity in n-C_{16} hydroconversion exhibit n_{as} values well above 2 [23]. This is typically evident from a significant fraction of multi-branched and cracked products at low conversion.

We analyzed the isomers distribution at low (4%), medium (33%) and high (66%) n-C_{16} conversion. Fig. 3 depicts the distribution of

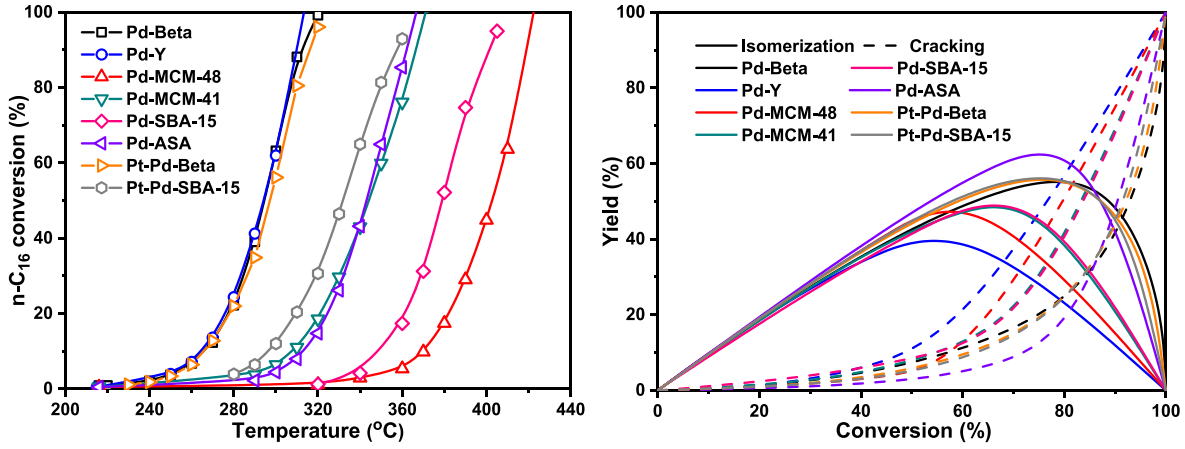

Fig. 2. Conversion of n- C_{16} as a function of the reaction temperature for zeolites and mesoporous silicas (left) and product yield distribution as a function of n-hexadecane conversion (right). Conditions: WHSV = 10 $g_{n\text{-}C16}\ g_{cat}^{-1}h^{-1}$, H_2/n-hexadecane = 20, P = 60 bar,~ 1 wt% Pd).

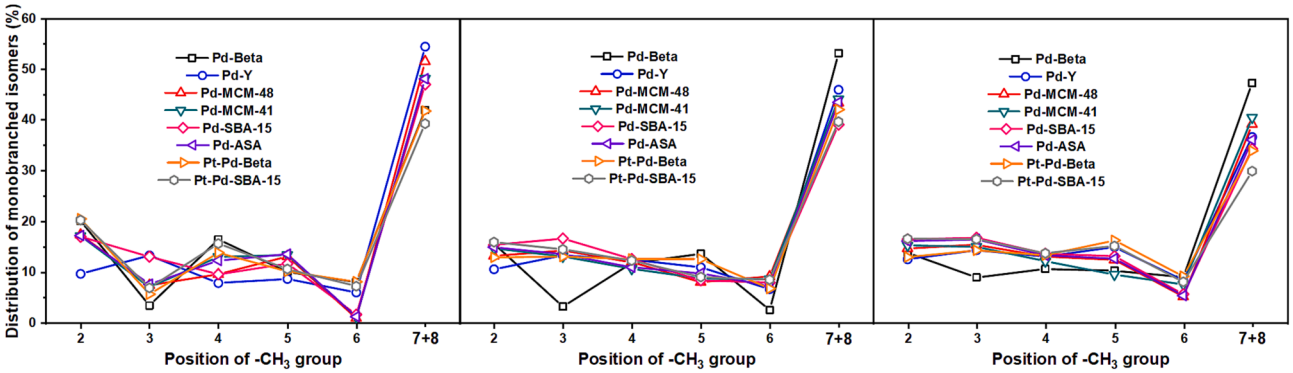

Fig. 3. Distribution of mono-branched C_{16} isomers at n-C_{16} conversion levels of 4% (left), 33% (center) and 66% (right).

mono-branched isomers at these n-C_{16} conversion levels. These distributions show a similar dependence on the methyl position at a given conversion. It should be noted that 7-methylpentadecane (7-meC15) and 8-methylpentadecane (8-meC15) could not be well separated. The following observations can be made. At low conversion, there is a slight preference for the methyl branch to end up at the C_2 position compared to C_3-C_6 positions for all samples except for Pd-Y. Besides, the combined selectivity to 7-meC15 and 8-meC15 also indicates a preference for methyl branching at positions close to the center of the hydrocarbon. With increasing conversion, these differences become smaller, although there remains a slight preference for more central locations. At high conversion, the differences between the various catalysts are relatively small, Pd-Beta presenting a slightly different distribution. The group of Martens reported a strong preference for methyl branching at the C_2 position in n-C_{17} hydrocracking for a shape-selective Pt/ZSM-22, whereas Pt/USY presented a distribution quite similar to the one presented for Pt-Y in our study [24].

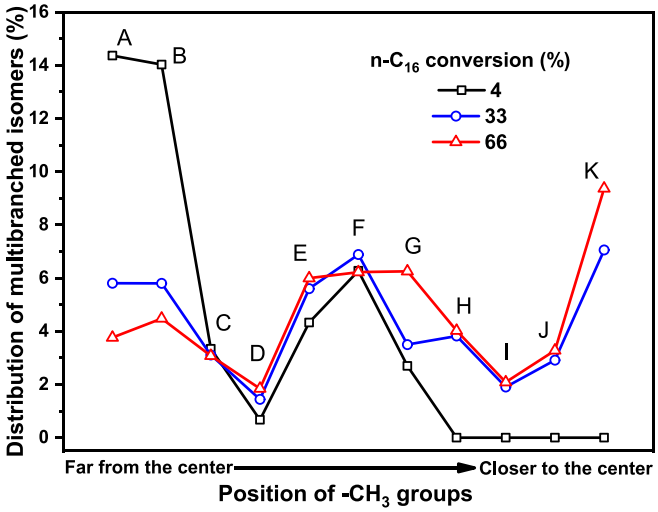

Fig. 4. Normalized distribution of di-branched C_{16} isomers at 4% (black line), 33% (blue line) and 66% (red line) of n-hexadecane hydroconversion for Pd-Y. A: (2,12-dimethyltetradecane + 3,12-dimethyltetradecane)/2, B: (2,13-dimethyltetradecane + 3,11-dimethyltetradecane)/2, C: (2,11-dimethyltetradecane + 4,11-dimethyltetradecane)/2, D: (3,7-dimethyltetradecane + 3,8-dimethyltetradecane + 3,9-dimethyltetradecane)/3, E: (2,10-dimethyltetradecane + 5,10-dimethyltetradecane + 6,9-dimethyltetradecane)/3, F: (2,7-dimethyltetradecane + 2,8-dimethyltetradecane + 2,9-dimethyltetradecane)/3, G: 4,10-dimethyltetradecane, H: (4,7-dimethyltetradecane + 4,8-dimethyltetradecane + 4,9-dimethyltetradecane)/3, I: (5,8-dimethyltetradecane + 5,9-dimethyltetradecane)/2, J: 6,7-dimethyltetradecane, K: 6,8-dimethyltetradecane. (For interpretation of the references to colour in this figure legend, the reader is referred to the web version of this article.)

We also analyzed the di-branched isomers distribution at similar conversion levels. These distributions are shown for Pd-Y in Fig. 4. The identification of these isomers was done in accordance with the elution sequence reported in the literature [25]. The values depicted in Fig. 4 are normalized distributions, considering that several isomers may elute at the same time, even at very low concentrations. As deconvolution into contributions of individual isomers was not possible, group values were determined by the total calculated molar amount for each peak divided by the number of isomer species represented by the peak. The groups are denoted in accordance with one or both methyl groups being located at the terminal end or closer-to-the-center positions of the tetradecane chain. The center is the C_7 position of this chain.

At a n-C_{16} conversion of 4%, the distribution is dominated by di-branched isomers containing both methyl groups far from the center, while there are less di-branched isomers with one methyl group at a terminal position and the other one approaching the center of the chain. At higher conversion levels, the amount of these latter isomers remains relatively constant, whereas the isomers with methyl groups adjacent to the center of the chain are observed in larger amounts than those with methyl groups at terminal positions. All the catalysts present a very similar distribution of di-branched isomers at low, medium and high n-C_{16} conversion levels (Fig. 5), suggesting that, in the absence of shape selectivity, the hydroconversion mechanism follows the same isomerization path for each sample independent of their topology, pore size and balance between metal and acid sites.

The product distribution of cracked hydrocarbons for Pd-Y, Pd-Beta, Pt-Pd-Beta and Pt-Pd-SBA-15 at n-C_{16} conversion levels of 4%, 33% and 66% are plotted in Fig. 6. In general, all the samples present comparable cracking patterns in accordance to the isomerization pathways discussed above. At low conversion, the samples exhibit an asymmetric 'M' shaped cracked product distribution in which the amount of lighter products in the C_4-C_6 range is larger than those in the C_8-C_{10} range, likely obtained from the cracking of ααγ-tri-branched isomers containing methyl groups at terminal positions of the chain, 2,2,4-trimethyltridecane for example. As dehydrogenation is thermodynamically favored at low pressures and high temperatures [26], low alkene coverage can be expected at this n-C_{16} conversion level (corresponding to low temperature) [27], disrupting the balance between acid and metal functions. The valley observed in the distribution between C_8 and C_{10} can be associated with the absence of di-branched isomers containing one methyl group located at carbon 4, 5 or 6 of the chain, which can evolve to ααγ-tri-branched isomer precursors via additional type B rearrangements and methyl shifts. Even if type A isomerization is generally considered to be considered substantially faster than type B isomerization, still preferred branching positions can be obtained depending on the attained degree of conversion [28].

At a n-C_{16} conversion of 33%, the distribution becomes more symmetric and the 'M' shape is mostly lost. At the highest n-C_{16} conversion of 66%, the typical bell-shaped distribution is obtained, approaching the

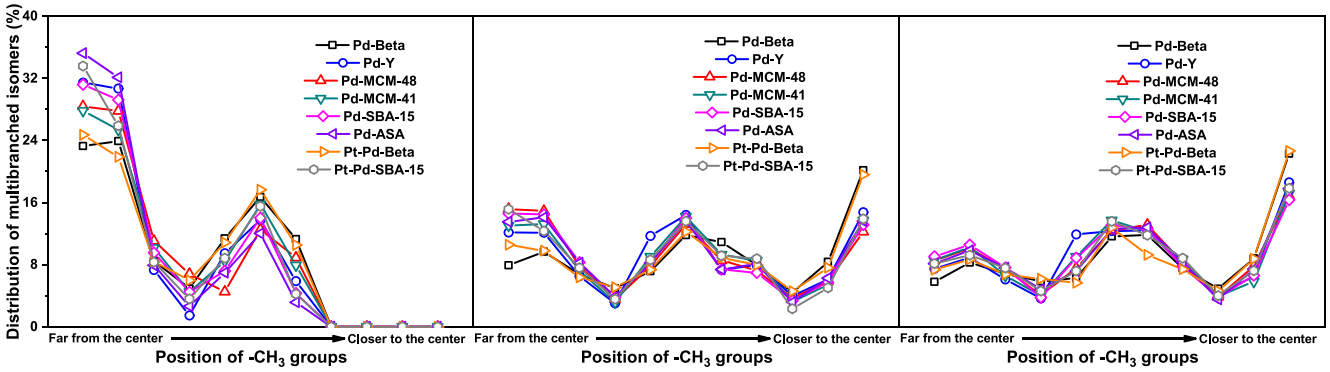

Fig. 5. Distribution of di-branched C_{16} isomers at n-C_{16} conversion levels of 4% (left), 33% (center) and 66% (right).

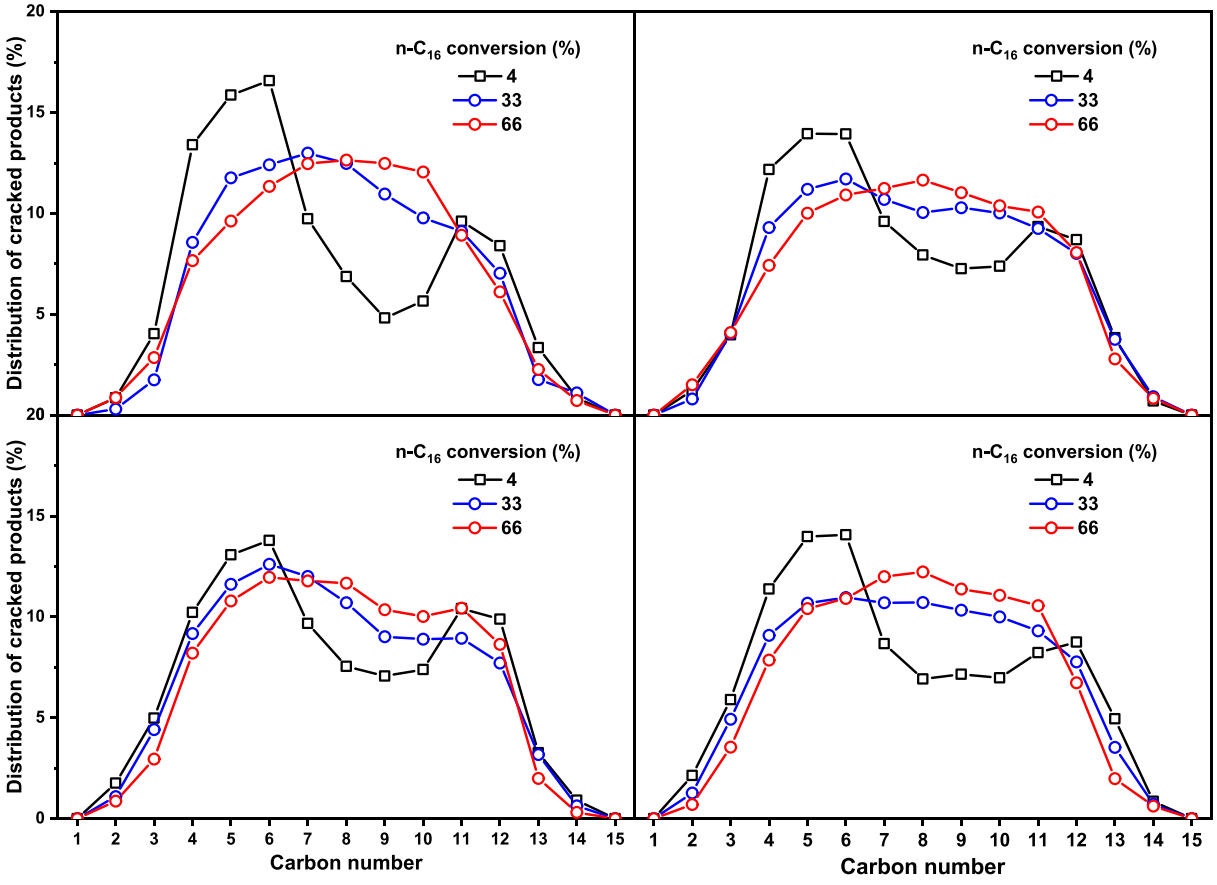

Fig. 6. Distribution of cracked products of Pd-Y (top, left), Pt-Pd-SBA-15 (top, right), Pd-Beta (bottom, left) and Pt-Pd-Beta (bottom, right) at increasing n-hexadecane conversion.

expected cracking pattern normally observed for a reaction operating in the ideal hydroconversion regime. This is also in accordance with the increasing prevalence observed for 6,7-dimethyltetradecane and 6,8-dimethyltetradecane in the isomers distribution. Similar C_3 and C_{13} amounts for all samples with increasing n-C_{16} conversion points out ααγ-tri-branched isomers cracking predominance over αα- and αγ-di-branched isomers cracking [29]. While Pd-SBA-15 presents an asymmetric distribution of cracked products shifted to lighter products, the addition of Pt (Pt-Pd-SBA-15) results in a cracked product distribution comparable to the one expected for ideal hydrocracking (Figure S7). Comparable differences in the distribution were observed between Pd-Beta and Pt-Pd-Beta (Fig. 6 and Figure S7). It has been reported in the literature [14] that some degree of secondary cracking takes place in catalysts containing one-dimensional mesopores, when the hydrogenation function is not strong enough, which is likely associated with a longer residence time of olefinic intermediates [30]. In addition, independent of the catalyst, the molar ratio of branched to total species in the C_4 to C_{13} fraction shows an increasing amount of branched species with respect to the fraction of n-paraffins at increasing conversion (Fig. 7). This points to secondary isomerization, meaning the occurrence of skeletal rearrangement after the primary cracking event. It is expected that type A and B ß-scission events would lead to similar iso/(iso + normal) values for each carbon number. An effect of the Brønsted acidity and, in particular, the acid site density can also be perceived, considering that zeolites have more acid sites than amorphous silica-alumina and aluminated (mesoporous) silica.

We also investigated the performance of some of these catalysts (Pd-Y, Pd-MCM-41, Pd-MCM-48 and Pd-SBA-15) in the hydroconversion of

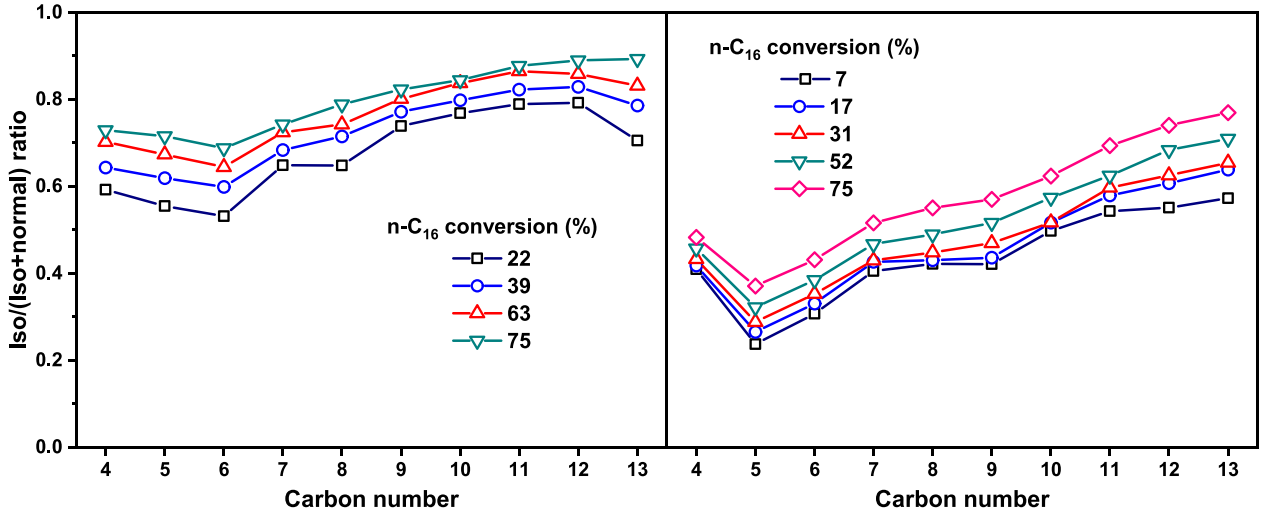

Fig. 7. Molar ratio of isomers from cracked products to total cracked products at increasing n-C_{16} conversion for Pd-Beta (left) and Pd-SBA-15 (right).

n-heptane (n-C_7). Using this lighter alkane as the reactant simplifies the analysis of mono- and di-branched isomers [31]. The n-C_7 experiments were performed at a H_2/n-C_7 molar ratio of 24 and a pressure of 30 bar. The n-C_7 conversion is given as a function of the temperature in Figure S8, while the product distributions are depicted in Figure S9. Similar to the n-C_{16} data, the more acidic zeolite-derived Pd-Y catalyst is substantially more active than the ordered mesoporous silica-based catalysts. Nevertheless, all these catalysts present very similar yields of cracked products as a function of the n-C_7 conversion.

Fig. 8 presents data on the mono- and di-branched isomers as a function of the n-C_7 conversion. The contribution of tri-branched isomers is very small, while typically mono-branched isomers make up most of the isomers. Fig. 8a shows that, except at low n-C_7 conversion, the 3-methylhexane/2-methylhexane (3-me/2-me) ratio follows the equilibrium 3-me/2-me ratios [32]. These equilibrium ratios vary for the different samples with n-C_7 conversion due to the different activities. At low n-C_7 conversion, there is a preference for 3-methylhexane, which can be explained by its higher probability of formation from any of the heptene secondary carbenium ions in comparison to the probability of 2-methylhexane formation. Interestingly, the decrease in the 3-me/2-me ratio to close-to-equilibrium values with conversion is much more pronounced for Pd-MCM-41 and Pd-MCM-48 than for Pd-Y and Pd-SBA-15. Iglesia and co-workers also reported that 3-me/2-me ratios followed equilibrium values for zeolites with sufficiently large pores, while the 2-me isomer was preferentially observed for 10MR zeolites, which can be due to differences in adsorption thermodynamics or diffusivity. Fig. 8b displays the selectivity to di-branched isomers. Although no thermodynamic data are available to calculate equilibrium values, it is reasonable to infer from these trends that 2,3-dimethylpentane is formed from 2-me and 3-me, followed by their isomerization to the other three possible di-branched isomers. These and even more reactive tri-branched isomers are the isomers that can undergo β-scission upon dehydrogenation and protonation.

Clearly, for the subset of catalysts tested in n-C_7 hydroconversion, no preferential sieving of particular isomers is observed. This is not surprising given the relatively small size of the involved mono- and di-branched isomers formed. The preference for 2,3-dimethylpentane formation at low n-C_7 conversion is related to the preferential formation of 3-methylhexene over 2-methylhexene from heptenes. Therefore, no clear preferential formation of isomers with terminal branching could be observed for the shorter n-heptane compared to n-hexadecane hydroconversion. Moreover, no trapping of particular di-branched isomers, which would lead to long residence times and substantial secondary cracking [23,31], as encountered in 10MR zeolites with a 3D topology like ZSM-5 is observed for these catalysts in which the acid sites reside in relatively large pores. From the n-C_{16} data, it follows that, at low conversion, the cracked products distribution displays a distinct 'M' shape, which can be linked to the observed preference of di-branched isomers

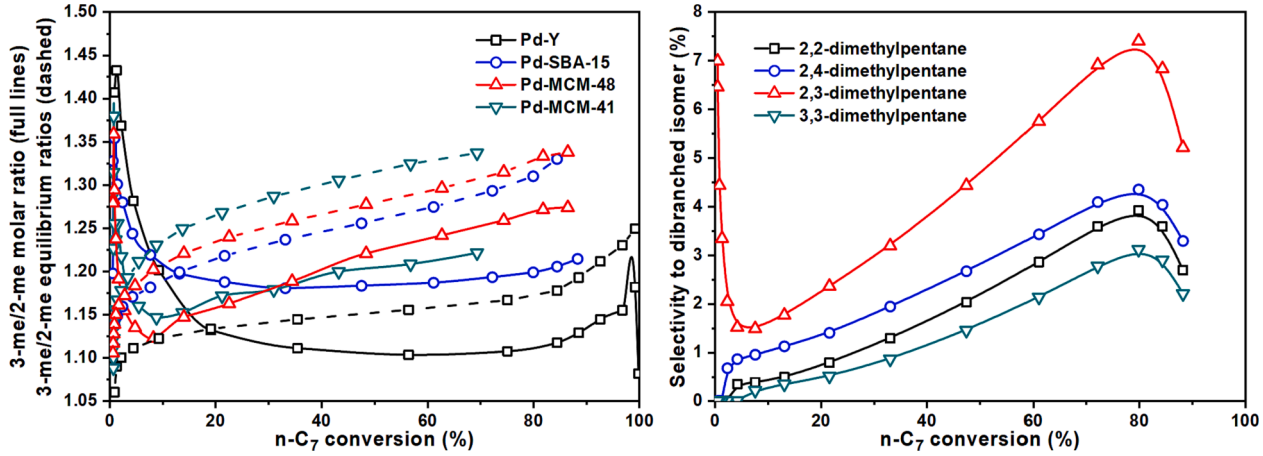

Fig. 8. (left) Experimental 3-me/2-me ratios (full lines) and equilibrium 3-me/2-me ratios (dashed lines) for Pd-Y, Pd-SBA-15, Pd-MCM-41 and Pd-MCM-48 and (right) selectivity to di-branched isomers for Pd-SBA-15 during n-C_7 hydroconversion.

with branches at the terminal end of the hydrocarbon. Others have also reported preferential formation of isomers with methyl branches located in terminal positions of the hydrocarbon in the context of pore-mouth catalysis [33–35]. This refers to preferential conversion of hydrocarbons that only partially enter the zeolite pores at the surface of the zeolite crystals. This phenomenon is usually discussed for hydrocracking of long-chain hydrocarbons in 10MR zeolites with a one-dimensional pore system such as TON and MTT [31] and at high conversion [34]. Here, we have presented data showing that di-branched isomers with methyl branches at terminal positions also form on other zeolites (zeolite Y, Beta) and even mesoporous materials containing much larger pores, suggesting that restricted diffusion of the reaction intermediates in small zeolite pores is not the cause of the observed selectivity trends. As a consequence, the cracked product distribution at relatively low conversion shows the distinct 'M' shape. At higher n-C_{16} conversion, the usual preference for the methyl groups at central positions in di-branched monomers is achieved, which can explain the shift to a symmetric cracked product distribution.

4. Conclusions

A number of large-pore zeolites, amorphous silica-alumina and aluminated ordered mesoporous silicas with varying acidity, topology and pore size were loaded with Pd or PtPd by (sequential) wet impregnation and evaluated for their catalytic performance in bifunctional hydroconversion of n-C_{16}. Analysis of the mono-branched isomers distribution showed a preference for the methyl branch at central positions at low n-C_{16} conversion. The distribution of di-branched isomers was dominated at low conversion by isomers containing the methyl groups located far from the center of the tetradecane chain. This distribution is consistent with the 'M' shaped cracked product distribution at low reactant conversion. With increasing n-C_{16} conversion, there is a clear shift in the di-branched isomers distribution in which isomers with methyl groups at positions closer to the center of the chain become dominant. This leads to the usually observed symmetric cracked product distribution belonging to ideal hydrocracking. Complementary n-C_7 hydroconversion measurements were performed in order to probe for similar peculiarities for a simpler reaction. A clear preference for isomers with terminal branching could not be determined as experimental mono-branched isomers ratios followed equilibrium values and no preferential sieving of certain isomers was observed. Overall, this investigation shows that some of the peculiarities normally associated with pore mouth catalysis of long-chain alkanes during hydroconversion in medium-pore zeolites are also observed for acidic supports with pores large enough to exclude diffusional restrictions of the hydrocarbons.

CRediT authorship contribution statement

Douglas Romero: Conceptualization, Writing – original draft, Methodology, Investigation, Formal analysis. **Marcello Rigutto:** Conceptualization, Writing – review & editing, Supervision. **Emiel J.M. Hensen:** Conceptualization, Writing – review & editing, Supervision, Funding acquisition.

Declaration of Competing Interest

The authors declare that they have no known competing financial interests or personal relationships that could have appeared to influence the work reported in this paper.

Data availability

Data will be made available on request.

Acknowledgements

D.R. and E.J.M.H, acknowledge Shell Global Solutions International for financial support, A.M. Elemans-Mehring for ICP-OES analysis, and the Soft Matter Cryo-TEM Research Unit of Eindhoven University of Technology for access to TEM facilities.

Appendix A. Supplementary material

Supplementary data to this article can be found online at https://doi.org/10.1016/j.fuel.2023.130264.

References

[1] A.G. Bridge, U.K. Mukherjee, Isocracking-Hydrocracking for superior fuels and lubes production, in: Handb. Pet. Refin. Process., 2004: pp. 3–22.
[2] Weitkamp J. Catalytic Hydrocracking-Mechanisms and Versatility of the Process. ChemCatChem 2012;4:292–306. https://doi.org/10.1002/cctc.201100315.
[3] Weitkamp J, Jacobs PA, Martens JA. Isomerization and hydrocracking of C9 through C16 n-alkanes on Pt/HZSM-5 zeolite. Appl Catal 1983;8:123–41. https://doi.org/10.1016/0166-9834(83)80058-X.
[4] Knaeble W, Carr RT, Iglesia E. Mechanistic interpretation of the effects of acid strength on alkane isomerization turnover rates and selectivity. J Catal 2014;319:283–96.
[5] Weitkamp J, Schulz H. Olefinic intermediates in catalytic hydrocracking of paraffins. J Catal 1973;29:361–6. https://doi.org/10.1016/0021-9517(73)90241-8.
[6] Weisz PB. Polyfunctional Heterogeneous Catalysis. Adv Catal 1962;13:137–90.
[7] Zecevic J, Vanbutsele G, De Jong KP, Martens JA. Nanoscale intimacy in bifunctional catalysts for selective conversion of hydrocarbons. Nature 2015;528:245–54. https://doi.org/10.1038/nature16173.
[8] Cheng K, Wal LI, Yoshida H, Oenema J, Harmel J, Zhang Z, et al. Impact of the Spatial Organization of Bifunctional Metal-Zeolite Catalysts on the Hydroisomerization of Light Alkanes. Angew Chemie 2020;132:3620–8. https://doi.org/10.1002/ange.201915080.
[9] Oenema J, Harmel J, Vélez RP, Meijerink MJ, Eijsvogel W, Poursaeidesfahani A, et al. Influence of Nanoscale Intimacy and Zeolite Micropore Size on the Performance of Bifunctional Catalysts for n-Heptane Hydroisomerization. ACS Catal 2020;10:14245–57. https://doi.org/10.1021/acscatal.0c03138.
[10] Harmel J, Van Der Wal LI, Zečević J, De Jongh PE, De Jong KP. Influence of intimacy for metal-mesoporous solid acids catalysts for: N -alkanes hydroconversion, Catal. Sci Technol 2020;10:2111–9. https://doi.org/10.1039/c9cy02510c.
[11] Zečević J, Van Der Eerden AMJ, Friedrich H, De Jongh PE, De Jong KP. Heterogeneities of the nanostructure of platinum/zeolite y catalysts revealed by electron tomography. ACS Nano 2013;7:3698–705. https://doi.org/10.1021/nn400707p.
[12] Martens JA, Souverijns W, Verrelst W, Parton R, Froment GF, Jacobs PA. Selective Isomerization of Hydrocarbon Chains on External Surfaces of Zeolite Crystals. Angew Chemie - Int Ed 1995;34(22):2528–30.
[13] Bok TO, Andriako EP, Knyazeva EE, Ivanova II. Engineering of zeolite BEA crystal size and morphology: Via seed-directed steam assisted conversion. RSC Adv 2020;10:38505–14. https://doi.org/10.1039/d0ra07610d.
[14] Romero DE, Rigutto M, Hensen EJM. Influence of the size, order and topology of mesopores in bifunctional Pd-containing acidic SBA-15 and M41S catalysts for n-hexadecane hydrocracking. Fuel Process Technol 2022;232:48. https://doi.org/10.1016/j.fuproc.2022.107259.
[15] Holmberg BA, Wang H, Yan Y. High silica zeolite Y nanocrystals by dealumination and direct synthesis. Microporous Mesoporous Mater 2004;74(1-3):189–98.
[16] Torres-Rodríguez M, Gutiérrez-Arzaluz M, Mugica-Álvarez V, Aguilar-Pliego J, Pergher S. Alkylation of Benzene with Propylene in a Flow-Through Membrane Reactor and Fixed-Bed Reactor: Preliminary Results. Materials (Basel) 2012;5:872–81. https://doi.org/10.3390/ma5050872.
[17] Sangchoom W, Mokaya R. High temperature synthesis of exceptionally stable pure silica MCM-41 and stabilisation of calcined mesoporous silicas via refluxing in water. J Mater Chem 2012;22:18872. https://doi.org/10.1039/c2jm33837h.
[18] Xia Y, Mokaya R. Mesoporous MCM-48 aluminosilica oxynitrides: Synthesis and characterization of bifunctional solid acid-base materials. J Phys Chem C 2008;112:1455–62. https://doi.org/10.1021/jp077578g.
[19] Zhao D, Huo Q, Feng J, Chmelka BF, Stucky GD. Nonionic triblock and star diblock copolymer and oligomeric sufactant syntheses of highly ordered, hydrothermally stable, mesoporous silica structures. J Am Chem Soc 1998;120:6024–36. https://doi.org/10.1021/ja974025i.
[20] Guisnet M. "Ideal" bifunctional catalysis over Pt-acid zeolites. Catal Today 2013;218–219:123–34. https://doi.org/10.1016/j.cattod.2013.04.028.
[21] Batalha N, Pinard L, Pouilloux Y, Guisnet M. Bifunctional hydrogenating/acid catalysis: Quantification of the intimacy criterion. Catal Letters 2013;143:587–91. https://doi.org/10.1007/s10562-013-1003-9.
[22] Batalha N, Pinard L, Bouchy C, Guillon E, Guisnet M. N-Hexadecane hydroisomerization over Pt-HBEA catalysts. Quantification and effect of the intimacy between metal and protonic sites. J Catal 2013;307:122–31. https://doi.org/10.1016/j.jcat.2013.07.014.

[23] Romero D, Rohling R, Meng L, Rigutto M, Hensen EJM. Shape selectivity in linear paraffins hydroconversion in 10-membered-ring pore zeolites. J Catal 2021;394:284–98. https://doi.org/10.1016/j.jcat.2020.11.007.
[24]] J. a. Martens, W. Souverijns, W. Verrelst, R. Parton, G.F. Froment, P. a. Jacobs, Selective Isomerization of Hydrocarbon Chains on External Surfaces of Zeolites Crystals, Angew. Chem. Int. Ed. Engl. 34 (1995) 2528–2530.
[25] Claude MC, Vanbutsele G, Martens JA. Dimethyl Branching of Long n-Alkanes in the Range from Decane to Tetracosane on Pt / H – ZSM-22 Bifunctional Catalyst. J Catal 2001;203:213–31. https://doi.org/10.1006/jcat.2001.3325.
[26] Eliseev NA, Sterligov OD, Isagulyants GV. Thermodynamic parameters of dehydrogenation reactions of normal paraffins with a C10–C15 hydrocarbon composition to olefins. Russ Chem Bull 1987;36(4):674–7.
[27] Maesen TLM, Calero S, Schenk M, Smit B. Alkane hydrocracking : shape selectivity or kinetics ? J Catal 2004;221:241–51. https://doi.org/10.1016/j.jcat.2003.07.003.
[28] Weitkamp J, Farag H. Isomerization of the Methylnonanes and 2-methyloctane on a bifunctional zeolite catalyst. Acta Phys Chem 1978;24:327–33.
[29] J. a. Martens, P. a. Jacobs, J. Weitkamp, Attemps to rationalize the distribution of hydrocracked products. I qualitative description of the primary hydrocracking modes of long chain paraffins in open zeolites, Appl. Catal. 20 (1986) 239–281.
[30] J. Weitkamp, P.A. Jacobs, J. a. Martens, Isomerization and hydrocracking of C9 through C16 n-alkanes on Pt/HZSM-5 zeolite, Appl. Catal. 8 (1983) 123–141. https://doi.org/10.1016/0166-9834(83)80058-X.
[31] Noh G, Zones SI, Iglesia E. Isomer sieving and the selective formation of terminal methyl isomers in reactions of linear alkanes on one-dimensional zeolites. J Catal 2019;377:255–70. https://doi.org/10.1016/j.jcat.2019.07.022.
[32] R.A. Alberty, C.A. Gehrig, Standard Chemical Thermodynamic Properties of Alkane Isomer Groups, J. Phys. Chem. Ref. Data. 13 (1984) 1173–1197. https://doi.org/10.1063/1.555726.
[33] Martens JA, Vanbutsele G, Jacobs PA, Denayer J, Ocakoglu R, Baron G, et al. Evidences for pore mouth and key-lock catalysis in hydroisomerization of long n-alkanes over 10-ring tubular pore bifunctional zeolites. Catal Today 2001;65:111–6. https://doi.org/10.1016/S0920-5861(00)00577-0.
[34] Souverijns W, Martens JA, Froment GF, Jacobs PA. Hydrocracking of isoheptadecanes on Pt/H-ZSM-22: An example of pore mouth catalysis. J Catal 1998;174:177–84. https://doi.org/10.1006/jcat.1998.1959.
[35] C.S. Laxmi Narasimhan, J.W. Thybaut, G.B. Marin, J.A. Martens, J.F. Denayer, G. V. Baron, Pore mouth physisorption of alkanes on ZSM-22: Estimation of physisorption enthalpies and entropies by additivity method, J. Catal. 218 (2003) 135–147. https://doi.org/10.1016/S0021-9517(03)00069-1.